



Ambient Temperature Effects on the Spring and Autumn Somatic Growth Trajectory Show Plasticity in the Photoneuroendocrine Response Pathway in the Tundra Vole

Mattis Jayme van Dalum^{*,1,2}, Laura van Rosmalen^{†,‡,1}, Daniel Appenroth^{*},
Fernando Cazarez Marquez^{*}, Renzo T. M. Roodenrijs[†], Lauren de Wit[†], Roelof A. Hut[†]
and David G. Hazlerigg^{*}

^{*}Arctic Seasonal Timekeeping Initiative, Department of Arctic and Marine Biology, UiT—the Arctic University of Norway, Tromsø, Norway, [†]Chronobiology Unit, Groningen Institute for Evolutionary Life Sciences, University of Groningen, Groningen, The Netherlands, and [‡]The Salk Institute for Biological Studies, La Jolla, California

Abstract Seasonal mammals register photoperiodic changes through the photoneuroendocrine system enabling them to time seasonal changes in growth, metabolism, and reproduction. To a varying extent, proximate environmental factors like ambient temperature (T_a) modulate timing of seasonal changes in physiology, conferring adaptive flexibility. While the molecular photoneuroendocrine pathway governing the seasonal responses is well defined, the mechanistic integration of nonphotoperiodic modulatory cues is poorly understood. Here, we explored the interaction between T_a and photoperiod in tundra voles, *Microtus oeconomus*, a boreal species in which the main impact of photoperiod is on postnatal somatic growth. We demonstrate that postweaning growth potential depends on both gestational and postweaning patterns of photoperiodic exposure, with the highest growth potential seen in voles experiencing short (8h) gestational and long (16h) postweaning photoperiods—corresponding to a spring growth program. Modulation by T_a was asymmetric: low T_a (10 °C) enhanced the growth potential of voles gestated on short photoperiods independent of postweaning photoperiod exposure, whereas in voles gestated on long photoperiods, showing a lower autumn-programmed growth potential, the effect of T_a was highly dependent on postweaning photoperiod. Analysis of the primary molecular elements involved in the expression of a neuroendocrine response to photoperiod, thyrotropin beta subunit (*tsh β*) in the *pars tuberalis*, somatostatin (*srif*) in the arcuate nucleus, and type 2/3 deiodinase (*dio2/dio3*) in the mediobasal hypothalamus identified *dio2* as the most

1. These authors contributed equally to this work.
2. To whom all correspondence should be addressed: Mattis Jayme van Dalum, Arctic Seasonal Timekeeping Initiative, Department of Arctic and Marine Biology, UiT—the Arctic University of Norway, Framstredet 41, Tromsø 9037, Norway; e-mail: m.v.dalum@gmail.com.

Correction (August 2023): Since the original online publication, this article has been updated to correct the second and fifth authors' affiliations.

JOURNAL OF BIOLOGICAL RHYTHMS, Vol. XX No. X, Month 202X 1–15

DOI: 10.1177/07487304231190156

© 2023 The Author(s)



Article reuse guidelines: sagepub.com/journals-permissions

T_a -sensitive gene across the study, showing increased expression at higher T_a , while higher T_a reduced somatostatin expression. Contrastingly *dio3* and *tsh β* were largely insensitive to T_a . Overall, these observations reveal a complex interplay between T_a and photoperiodic control of postnatal growth in *M. oeconomus*, and suggest that integration of T_a into the control of growth occurs downstream of the primary photoperiodic response cascade revealing potential adaptivity of small herbivores facing rising temperatures at high latitudes.

Keywords seasonality, maternal photoperiodic programming, temperature, photoperiodic neuroendocrine system, pars tuberalis, hypothalamus, *Microtus oeconomus*, tundra vole, deiodinase, thyroid signaling, testosterone and somatic growth

In species living in temperate and boreal zones, the scheduling of growth, development, and reproduction is contingent on the annual cycle of seasonal environmental change stemming from Earth's orbit of the Sun. This has led to the evolution of seasonal synchronization mechanisms reliant on changes in the daily photoperiod as a synchronizer (Dardente et al., 2014; Hazlerigg and Simonneaux, 2015; Wood and Loudon, 2018). In addition, to a degree that varies between species, proximate factors such as nutritional status, ambient temperature (T_a), predation, and social interactions modulate seasonal scheduling, giving phenotypic plasticity in the face of year-to-year variation in environmental seasonality (Bronson, 1985, 2009; Visser et al., 2010).

It has been argued based on life-history considerations that modulatory effects conferring plasticity are likely to be of increased importance in smaller short-lived species (e.g., nonhibernating rodents) than in larger species that survive and reproduce over multiple years (e.g., cervids) (Bronson, 1988). Accordingly, we have focused on microtine rodents as a suitable group in which to explore interactions between photoperiod and nonphotic influences on seasonal physiology.

Voles of the genus *Microtus*, the most speciose mammalian genus, inhabit large distribution ranges from the equator to the high arctic (Brunhoff et al., 2003; Jaarola et al., 2004), thereby meeting a variety of seasonal environments. In most *Microtus* species living at temperate and high latitudes, breeding starts in spring and ends in autumn with considerable variation in the onset and offset of the breeding season between species, populations, and years (Balčiauskas et al., 2012; Ergon, 2007; Gliwicz, 1996; Tast, 1966). High vole population densities delay the breeding onset and reduce the probability of maturation (Ergon et al., 2001), whereas a high predation risk advanced the onset of the breeding season (Gliwicz, 2007). Ambient temperature serves as an additional time cue in some birds (Visser et al., 2009), and it interacts with photoperiod on the GnRH system in prairie voles (Kriegsfeld et al., 2000). Voles breed in cohorts with spring-born pups growing and maturing fast to

reach a high summer body mass and reproduce during the same breeding season. By contrast, pups born later in the season grow slower, maintain a lower body mass, overwinter in juvenile state, and sexually mature shortly before the onset of the next breeding season (Eccard and Herde, 2013; Gliwicz, 1996).

In the common vole (*Microtus arvalis*), we recently reported that photoperiodic experience in early life shapes postnatal reproductive development, preparing the voles for either rapid reproduction or overwintering. This developmental trajectory is determined by interactive effects of photoperiod exposure experienced in utero, via the maternal melatonin signal, and in the juvenile period, directly through the pup's own photoneuroendocrine system (Horton and Stetson, 1992; van Rosmalen et al., 2021). Furthermore, we have demonstrated that temperature influences on this response are associated with changes in thyroid hormone deiodinase gene (*dio2* and *dio3*) expression in the basal hypothalamus (van Rosmalen et al., 2021)—establishing a point of intersection with the photoperiodic response one step removed from proximate actions of photoperiod on thyroid stimulating hormone (*tsh β*) expression in the *pars tuberalis* (PT) of the pituitary gland (Dardente et al., 2014).

We have also begun to investigate photoperiodic influences in a species with a more northerly paleogeography, the tundra vole (*Microtus oeconomus*) (Conroy and Cook, 2000). In contrast to the common vole, early life photoperiod has a smaller impact on postnatal reproductive development in *M. oeconomus*, while there are clear photoperiodic influences on somatic growth during the juvenile period, not seen in *M. arvalis* (van Rosmalen et al., 2020). These results suggest that photoperiod controls the somatic and gonadal axes differently between the two species.

The interaction of photoperiod and other environmental factors with gonadal development is better understood (for review, see Hazlerigg and Simonneaux, 2015) than with body mass and energy metabolism. The growth hormone (GH) axis is one potential photoperiod-controlled pathway. GH-releasing hormone (GHRH) from the arcuate nucleus stimulates the

release of GH from the pituitary, but this is inhibited by somatostatin, also referred to as somatotropin release inhibiting factor (SRIF) (Dumbell et al., 2015). Somatostatin expression in the arcuate nucleus is strongly regulated by photoperiod in Siberian hamsters but the effects of other environmental factors such as ambient temperature remain to be investigated (Herwig et al., 2012; Petri et al., 2016).

In this study, our aim was 3-fold. First, we wished to extend our initial characterization of early life photoperiod influences on somatic growth in *M. oeconomus* to resolve between the effects of gestational and neonatal photoperiod. Second, by combined manipulation of photoperiod and ambient temperature, we sought to assess the extent to which photoperiodically programmed seasonal growth trajectories show plasticity. Finally, by analysis of gene expression in the basal hypothalamus and PT, we sought to determine the extent to which modulatory effects of temperature on juvenile growth reflect effects on the neuroendocrine machinery of the primary photoperiodic response.

MATERIALS AND METHODS

Animals and Experimental Procedures

All experimental procedures were carried out according to the guidelines of the animal welfare body (IvD) of the University of Groningen conform to Directive 2010/63/EU and approved by the Centrale Commissie Dierproeven (CCD) of the Netherlands (CCD license number: AVD1050020171566). Tundra or root voles (*M. oeconomus*) were obtained from four different areas in the Netherlands (van de Zande et al., 2000). The population has been kept in the laboratory as an outbred colony at the University of Groningen, which provided all voles used in this study. Adult and weaned voles were individually housed in transparent plastic cages (15 × 40 × 24 cm) provided with sawdust, dried hay, an opaque PVC tube, and ad libitum water and food (standard rodent chow; Altromin #141005). The experiments were carried out in temperature-controlled chambers in which ambient temperature (T_a) and photoperiod were manipulated as described below.

The voles used in the experiment (102 males) were gestated and born at 21 °C under either a short photoperiod (SP, 8 h of light/24 h: early breeding season, hereafter termed “spring-programmed”) or a long photoperiod (LP, 16 h of light/24 h: late breeding season, hereafter termed “autumn-programmed”) and weaned at an age of 21 days old. After weaning, voles were transferred to either 10 °C or 21 °C and a range of different photoperiods, a

laboratory equivalent to different seasonal conditions (Figure 1a). Postweaning photoperiods (postPPs) were (hours light: hours dark): 16L:8D, 14L:10D, 12L:12D, 10L:14D. Hence, spring-programmed voles experienced a postweaning increase in photoperiod, while autumn-programmed voles experienced a postweaning decrease in photoperiod. All voles were weighed when 7, 15, 21, 30, 42, and 50 days old.

Tissue Collection

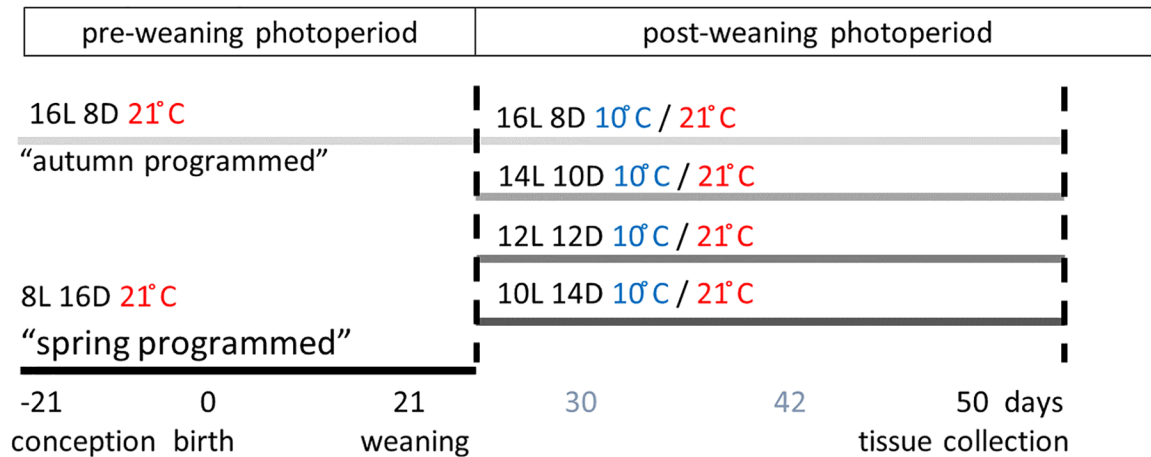
At the age of 50 days, and ~17h after lights-off, voles were sedated with CO₂ and then decapitated. Trunk blood was collected directly from each individual into heparinized tubes. Blood samples were left on ice until centrifugation (10 min, 2600 × g, 4 °C). Plasma was transferred to a clean tube and stored at –80 °C until hormonal assay. Whole brains were carefully dissected to include the proximate pituitary stalk including the PT. Within 5 min after decapitation, brains were slowly frozen on a brass block surrounded by liquid N₂. Brains were stored at –80 °C until proceeded to in situ hybridization. Reproductive organs were dissected, cleaned of fat, and wet masses of paired testes weight were measured (±0.0001 g).

Radioactive In Situ Hybridization

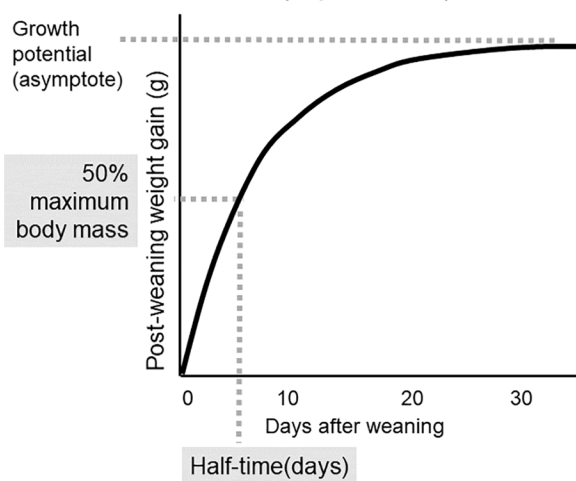
A detailed description of the in situ hybridization protocol can be found elsewhere (Lomet et al., 2018). Briefly, 20-µm coronal brain sections were cut on a cryostat in caudal to rostral direction, starting from the mammillary bodies to the optic chiasm, to cover the area of the hypothalamus and third ventricle. Sections were mounted onto pre-coated Superfrost Plus slides (Thermo scientific: ref J1800AMNZ) with 6-10 sections per slide and 10 slides per individual. Antisense riboprobes of rat *tshβ* (GenBank accession no. M10902, nucleotide position 47-412), *M. arvalis dio2* (GenBank accession no. JF274709, position 1-775) and *M. arvalis dio3* (GenBank accession no. JF274710, position 47-412) were transcribed from linearized cDNA templates. Incorporation of 35^S-UTP (Perkin Elmer, Boston, MA, USA) was done with T7 polymerase (*dio2* and *dio3*) and T3 polymerase (*tshβ*), resulting in 0.5-1.5 × 10⁶ counts per minute per microliter, calculated to have 10⁶ counts/min/slide. All slides were fixed in paraformaldehyde, acetylated, and hybridized with radioactive probes overnight at 56 °C.

Slides were washed in sodium citrate buffer the next day to remove nonspecific probe and then

(a) Experimental design



(b) Growth curve (equation 1)



(c) Dose-response curve (equation 2)

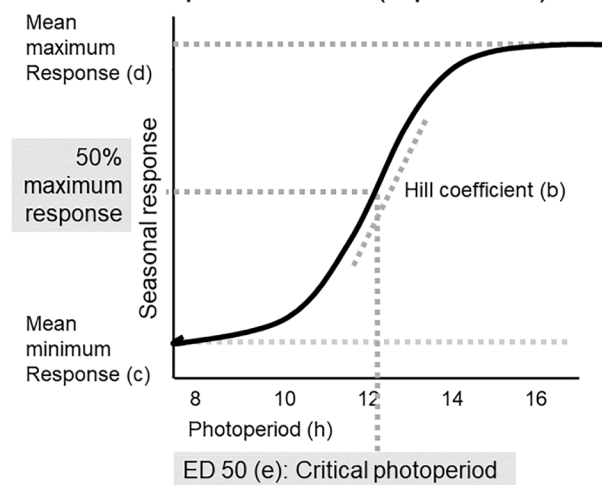


Figure 1. Experimental design and visualization of curve-fitting parameters. (a) Experimental design: conception, gestation, birth, and lactation took place under either 16 h of light (i.e., autumn-programmed) or 8 h of light (i.e., spring-programmed) at 21 °C. At the day of weaning (21 days old), voles from both preweaning photoperiods were transferred to four different postweaning photoperiods at either 10 °C or 21 °C resulting in eight different postweaning treatments. Tissue collections took place when voles were 50 days old. (b) Standard von Bertalanffy asymptotic growth function applied to the body mass data of each individual vole. (c) Four-parameter log-logistic function fitted to the mean seasonal response to photoperiod.

dehydrated in ethanol solutions, followed by air-drying. The slides were exposed to an autoradiographic film (Kodak, Rochester, NY, USA) for 9 days (*dio2* and *dio3*) or 11 days (*tshβ*) and developed with Carestream Kodak autoradiography GBX Developer/replenisher (P7042-1GA, Sigma) and fixer (P7167-1GA, Sigma). Films were scanned with an Epson Perfection V800 Photo scanner at 2400-dpi resolution along with a calibrated optical density strip (T2115C; Stouffer Graphic Arts Equipment Co., Mishawaka, IN, USA). Analysis of integrated optical density (IOD) was done with software ImageJ, version Fuji (NIH Image, Bethesda MD, USA). The

section with the strongest signal was selected to represent each animal.

Nonradioactive In Situ Hybridization

Nonradioactive in situ hybridization using digoxigenin-labeled riboprobes was performed to assess somatostatin (*srif*) expression in the arcuate nucleus of the mediobasal hypothalamus. Plasmids containing the rat somatostatin probe (135-465 of GenBank NM012659, 95% homology with *M. oeconomus* mRNA sequence, probe kindly provided by Dr. Paul Klosen)

was used to transcribe the probe from PCR-produced templates in the presence of digoxigenin-labeled nucleotides (Roche, Meylan, France).

To avoid background differences in the staining, the whole set of slides was stained at once. The sections were postfixed with 4% formaldehyde, acetylated for 10 min in 100-mM triethanolamine and 0.25% acetic anhydride, and delipidated with 0.1% Triton X-100. The tissue was then hybridized with 200-ng/mL of labeled antisense probe in 50% formamide, 5× saline sodium citrate (SSC), 5× Denhardt's solution, 250 µg/mL of baker's yeast tRNA, and 200-µg/mL herring sperm DNA for 14 h at 60 °C. Sequential stringency washes were performed at 55 °C with 5× SSC (5 min), 2× SSC (1 min) and 0.2× SSC 50% formamide (30 min), and finally 0.2× SSC (5 min) at room temperature. The digoxigenin tag was detected using an alkaline phosphatase-coupled anti-digoxigenin antibody (1:3000; Roche). Alkaline phosphatase activity was visualized with a mixture of nitro blue tetrazolium/bromo-chloro-indolyl phosphate and stopped 3 h later before the staining intensity reached saturation. Hybridization with corresponding sense probes gave no signal, indicating specificity of the antisense probe.

Micrographs were acquired with a slide scanner (Olympus, VS120, Tokyo, Japan), using a 20× objective. All pictures were taken in one session with identical lighting conditions for all voles. First, the arcuate nucleus region was extracted using Qupath (version 0.4.1., Bankhead et al., 2017) and then ImageJ was used to determine the mean intensity of the in situ hybridization signal using a fixed squared size.

Hormone Analysis

Plasma testosterone levels were measured in a mouse testosterone enzyme-linked immunosorbent assay according to manufacturer's instructions (ADI-900-065; Enzo Life Sciences, New York, NY, USA). Sensitivity: 5.67 pg/ml, intra-assay coefficient of variation: 10.8%, interassay coefficient of variation: 9.3%.

Fitting of Growth Curves

Postweaning growth in individual voles was modeled using a standard von Bertalanffy asymptotic growth function:

$$W_t = W_\infty * (1 - e^{-kt}), \quad (1)$$

where W_t is the weight at time t , W_∞ is the growth potential (asymptote; the theoretical maximum size which an individual will attain), and k is the rate constant for reaching the asymptotic potential. The half-time was calculated as the time taken to attain 50% of

the projected maximum weight. The day of weaning was set as $t=0$ and mass at $t=0$ was subtracted to give a zero baseline (Figure 1b). A summary of curve fits, giving W_∞ and half-times $(\ln[2])/k$, can be found in Table S1.

Calculation of Critical Photoperiod for Gene Expression Responses

Four-parameter log-logistic functions were fitted through the data to describe the response to photoperiod as a dose-response relationship.

$$y = d + \frac{(c-d)}{1 + \left(\frac{x}{e}\right)^b}. \quad (2)$$

In which b =slope parameter (hill coefficient), c =minimum, d =maximum, and e =50% maximal response, where ED50 is defined as the inflection point of the curve. Critical photoperiod (CP) was estimated by the ED50 from fitted dose-response curves (Figure 1c). All fitted dose-response curve parameters can be found in Table S2.

Analysis of Variance and Post Hoc Testing

The effects of postPP, T_a , and interactions were determined within spring- and autumn-programmed experimental groups using two-way analysis of variance (ANOVA). To detect differences in the growth rate between groups, we used repeated-measures ANOVAs. The effect of somatostatin expression and T_a on growth and body mass was tested using a generalized linear model.

Data were log transformed for *dio2*, *dio3*, paired testes mass, and testosterone. Where appropriate, post hoc testing was performed using Tukey's or Šidák's test. Statistical significance was determined at $p < 0.05$ and results in the text are given as mean ± standard error of the mean (SEM). For all variables except somatostatin curve fitting, statistical analyses and figures were generated using GraphPad Prism v9. Somatostatin curve fitting, statistical analysis, and regression plots were done in R studio (RStudio Team, 2020) using the packages tidyverse (Wickham et al., 2019), drc (Ritz et al., 2015), and lsmeans (Lenth, 2016).

RESULTS

We have measured the postweaning growth and gene expression response to photoperiod and temperature in either spring- or autumn-programmed voles. The experimental design is summarized in Figure 1a.

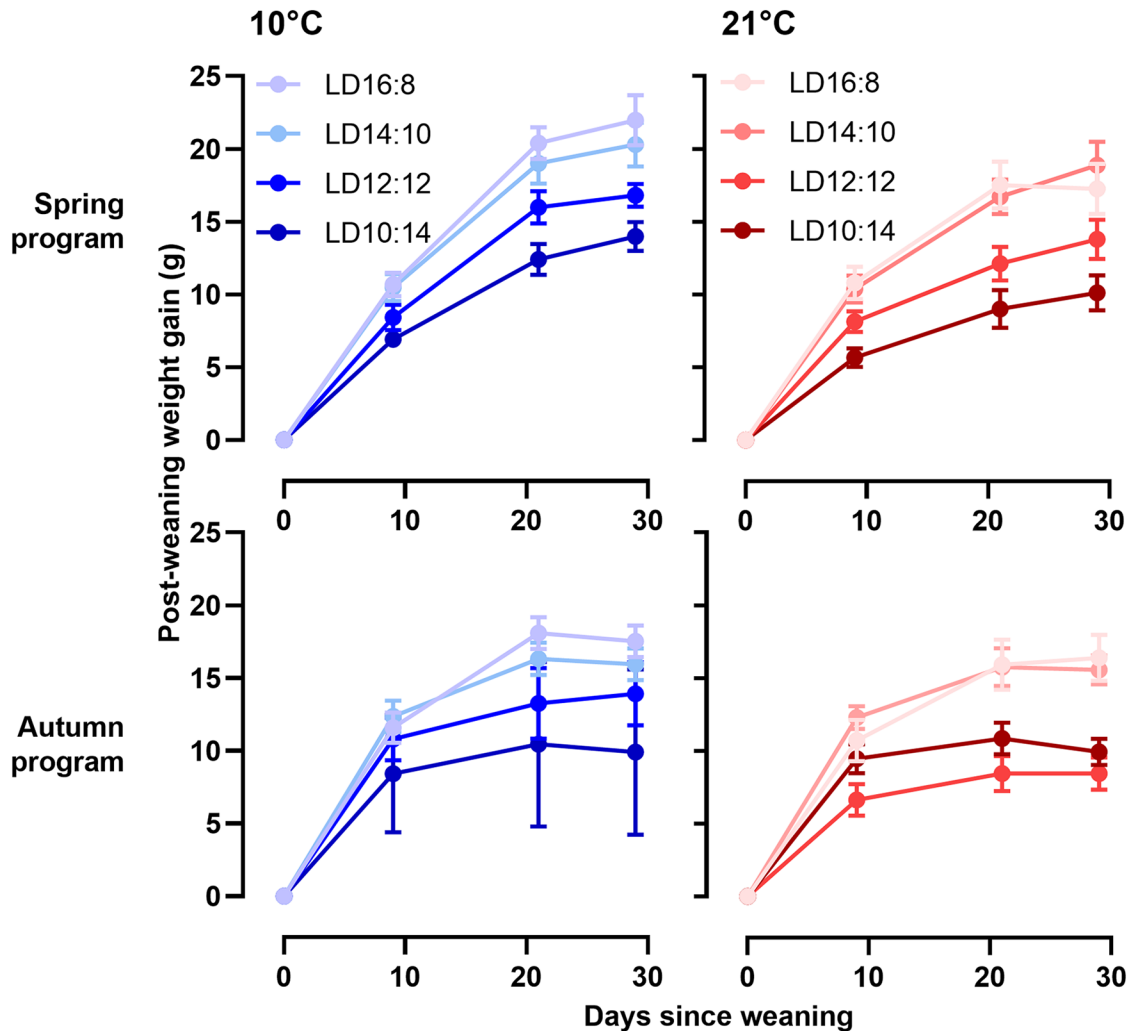


Figure 2. Postweaning growth curves in relation to photoperiod and ambient temperature. Postweaning growth curves for four different postweaning photoperiods at 10 °C (blue) or 21 °C (red) in both spring-programmed (LD8:16, top panel) and autumn-programmed (LD16:8, bottom panel) voles. Data are plotted as mean \pm SEM ($n=4-8$). Abbreviation: SEM = standard error of the mean.

Somatic Growth

Photoperiodic conditions during gestation and prior to weaning (spring and autumn program) had no significant effect on body mass recorded at weaning (spring voles 16.5 ± 0.33 g; autumn voles 17.4 ± 0.49 g, $t_{73}=1.58$, $p=0.12$).

The effects of ambient temperature (T_a) and postPP on postweaning somatic growth are summarized graphically in Figure 2, with curve fit parameters in Table S2. Overall, the growth potential, defined as the asymptotic weight in the von Bertalanffy function (Equation 1, Figure 1b), was consistently higher in spring-programmed voles (range: 7-58 g) than in autumn-programmed voles (range: 3-34 g) depending on postweaning conditions; postPP similarly had a strong influence on postweaning growth potential (spring, postPP:

$F_{3,52}=5.37$, $p=0.003$; autumn, postPP: $F_{3,33}=7.46$, $p<0.001$) with the highest asymptotic weights on LD16:8 being some 1.5-fold greater than corresponding values under LD10:14, across all combinations of preweaning photoperiod (prePP) and ambient temperatures. In spring-programmed voles, across all postPPs (Figure 3), low T_a (10 °C) in the postweaning phase increased growth potential by up to approximately 40% compared with voles raised after weaning at 21 °C (T_a : $F_{1,32}=9.21$, $p=0.004$, ns for $T_a \times$ postPP interaction). By contrast, T_a had no effect on growth potential in autumn-programmed voles (Figure 3).

Overall, postweaning half-times (in days, see Figure 1b) were significantly longer in spring (12.43 ± 1.15) than in autumn (5.04 ± 0.61) (prePP: $F_{1,97}=25.24$, $p<.0001$ and ns for T_a and $T_a \times$ prePP), indicating slower geometric approach to maximum

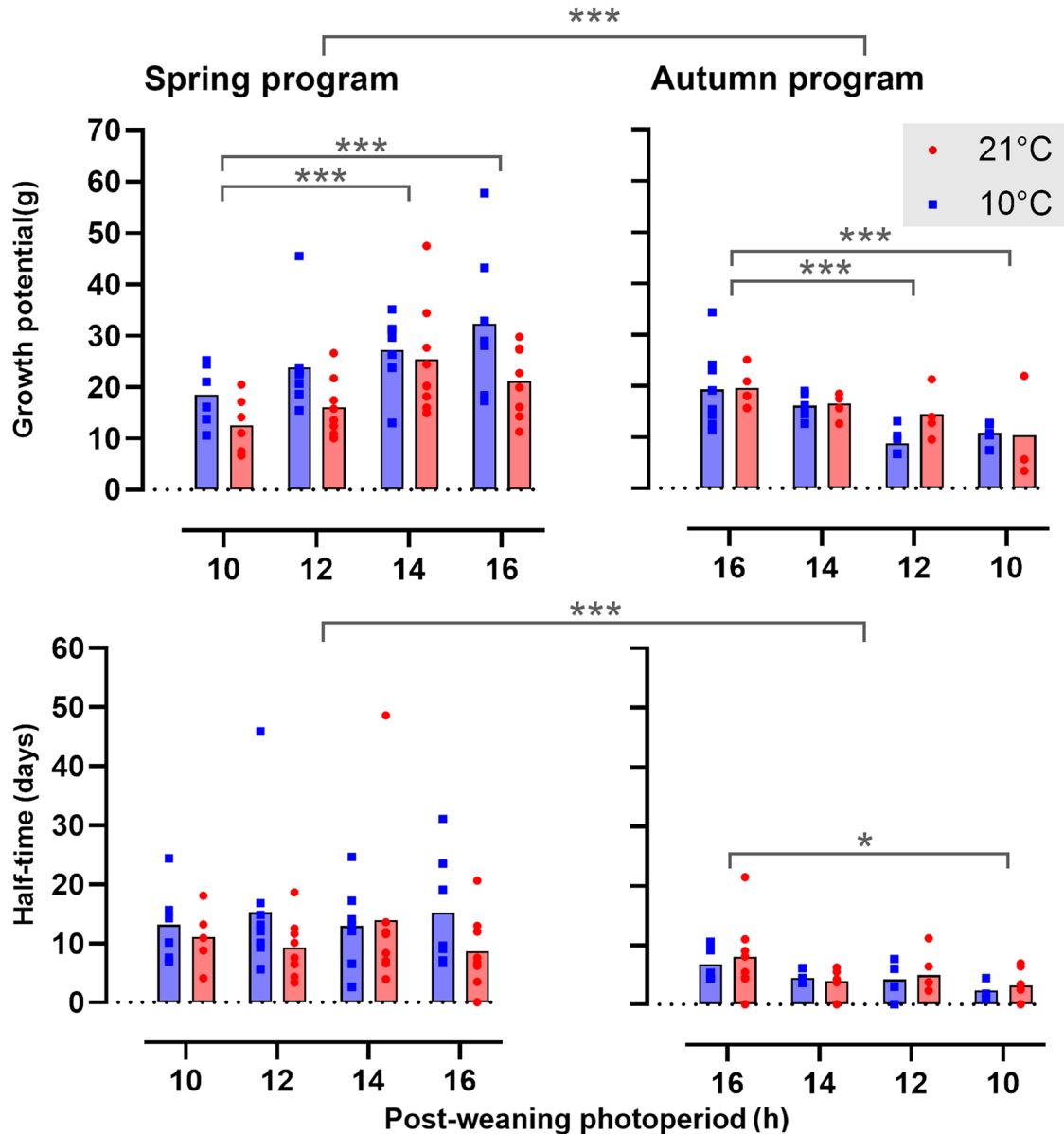


Figure 3. Mean growth potential and half-time in spring- and autumn-programmed voles. Growth potential is the asymptotic weight in the von Bertalanffy function, represented in the top panels, half-time (days) to reach the 50% maximum of the growth potential is shown in the lower panels for spring-programmed (left), and autumn-programmed (right) voles housed in postweaning ambient temperatures of either 10 °C (blue squares) or 21 °C (red circles). Significance levels are indicated: * $p < 0.05$. *** $p < 0.001$.

size in spring than in autumn. Only in autumn, short postPPs further reduced half-times (Figure 3, postPP: $F_{3,32} = 2.92$, $p = 0.05$, ns for T_a and $T_a \times$ postPP).

Photoneuroendocrine Pathway Gene Expression

The expression of *tsh β* in the PT followed a sigmoid relationship to postPP (Figure 4, Table S2) from which CP for the primary photoperiodic response could be estimated. In spring-programmed voles, this represents the CP for induction of a long day increase in *tsh β* expression, while in autumn-programmed voles, this represents the CP for short day suppression of *tsh β*

expression. In spring-programmed voles, CP was not significantly affected by T_a (10 °C CP_{spring} = 14.73, 95% confidence interval [CI] = 14.01-15.46, $R^2 = 0.76$; 21 °C CP_{spring} = 15.21, 95% CI = 14.93-15.49, $R^2 = 0.88$). Strong individual variation at LD14:10 at 10 °C led to a large spread around the estimated spring CP. In autumn-programmed voles, low T_a significantly decreased the CP for suppression of *tsh β* expression by about 1 h (10 °C CP_{autumn} = 14.38, 95% CI = 14.09-14.96, $R^2 = 0.93$; 21 °C CP_{autumn} = 15.38, 95% CI = 15.12-15.3; $R^2 = 0.93$ $p < 0.05$ for model comparison).

In contrast to *tsh β* , sigmoid model fits were poor descriptors of the patterns of *dio2* ($R^2 = 0.11-0.0$), *dio3*

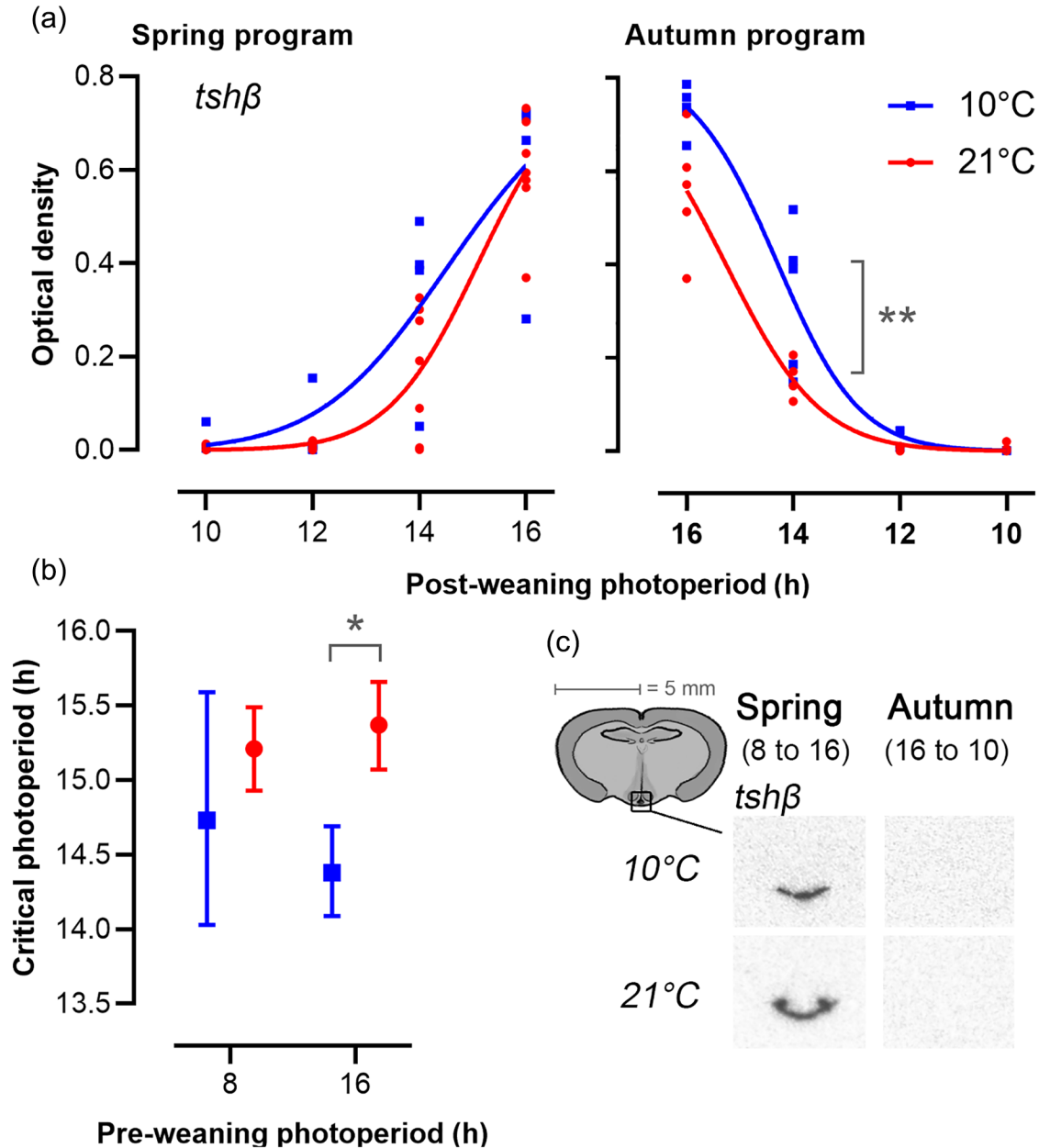


Figure 4. Expression of *tshβ* in the *pars tuberalis*. (a) Each data point represents optic density measurements from individual voles. Lines are best-fit curves for four-parameter log-logistic functions (Equation 2), as described in the methods. The left panels represent spring-programmed voles (gestated and raised to weaning under 8L) and the right panels represent autumn-programmed voles (gestated and raised to weaning under 16L) at 10 °C (blue squares) or 21 °C (red circles). All photoperiod treatments were significantly different from each other, except LD10:14 vs LD12:12 in both spring and autumn. (b) Critical photoperiod derived from fitted dose-response curves (Tables S1, S2) for *tshβ*; data are mean \pm 95% CL ($n=4-8$). (c) Representative images showing localization of mRNA by radioactive in situ hybridization for *tshβ* in the PT for the minimum and maximum expression levels during increasing (spring) and decreasing (autumn) photoperiods.

Significance levels are indicated: * $p < 0.05$. ** $p < 0.01$.

($R^2=0.47-0.60$), and somatostatin ($R^2=0.01-0.02$), gene expression across the postPP regimes (Figures 5 and 6, Table S2), but clear preweaning and postweaning effects were nonetheless observed. Overall *dio2* (Figure 5) expression was markedly higher in spring-programmed voles (0.06 ± 0.01) compared with autumn-programmed voles (0.02 ± 0.004), while the

inverse was observed for *dio3* (spring: 0.06 ± 0.01 , autumn: 0.24 ± 0.04).

Within spring-programmed voles, *dio2* was sensitive to postPP with the highest expression levels in LD16:8 voles being up to two orders of magnitude higher than levels in voles raised after weaning on LD10:14 (postPP: $F_{3,38}=6.06$, $p=0.002$). Across all

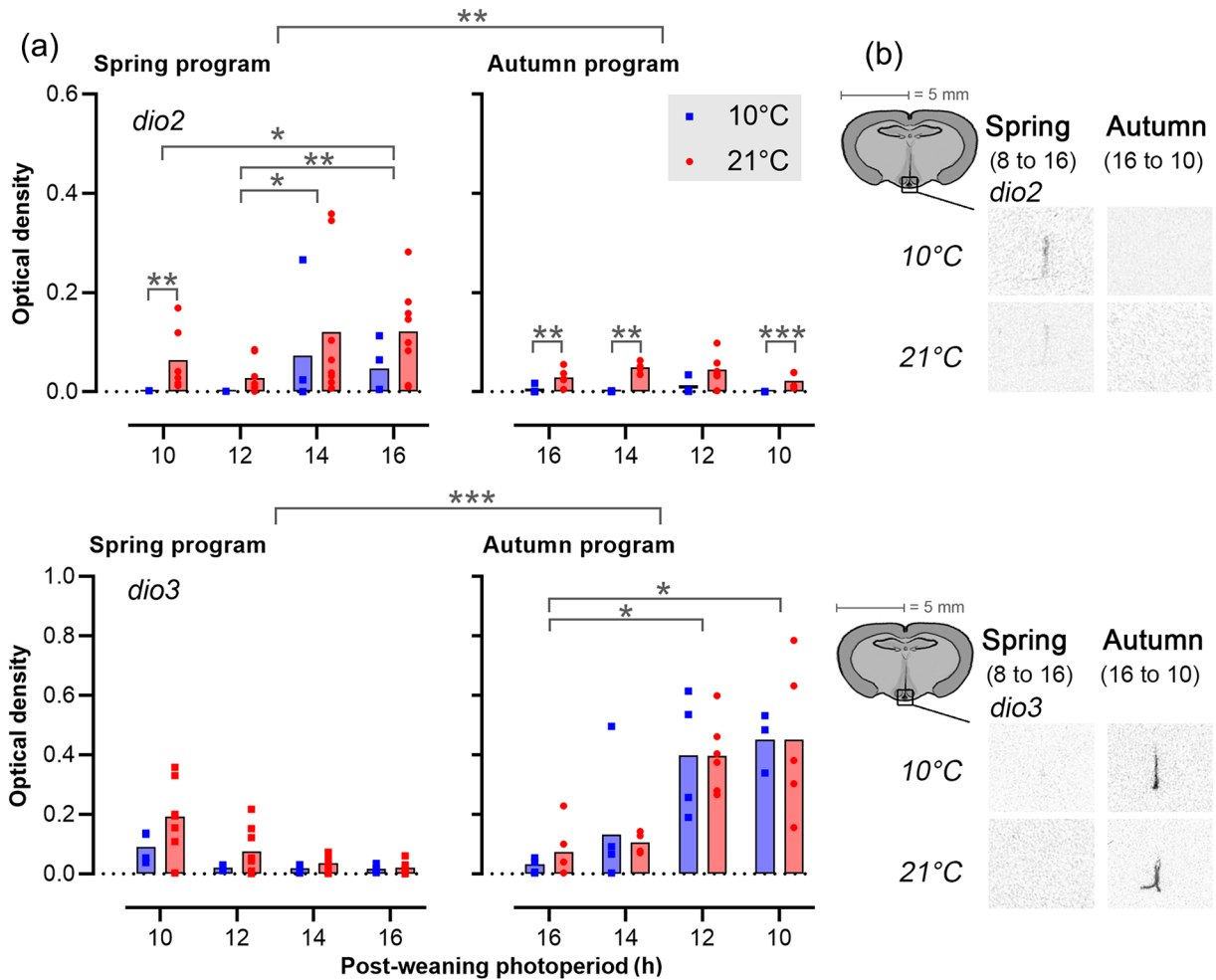


Figure 5. Expression of *dio2* and *dio3* in the tanycytes. (a) Bar plots showing *dio2* and *dio3* expression in tanycytes (mean, dots are individuals). The left panels represent spring-programmed voles (gestated and raised to weaning under 8L) and the right panels represent autumn-programmed voles (gestated and raised to weaning under 16L) at 10 °C (blue squares) or 21 °C (red circles). (b) Representative images showing localization of mRNA in the median eminence region for the minimum and maximum expression levels during increasing (spring) and decreasing (autumn) photoperiods.

Significant effects are indicated: * $p < 0.05$. ** $p < 0.01$. *** $p < 0.001$.

postPPs, spring-programmed voles raised after weaning at a higher T_a generally had higher *dio2* expression than their low T_a counterparts (T_a : $F_{1,38} = 26.17$, $p < 0.0001$). Although there was no significant postPP $\times T_a$ interaction under two-way ANOVA, the effect of T_a on spring program *dio2* expression was most apparent at short postPP, where expression appeared clamped at basal / background levels at 10 °C. In autumn-programmed voles, *dio2* expression was uniformly low across all postPPs, but a positive effect of increased T_a could still be observed (T_a : $F_{1,29} = 30.42$, $p < 0.0001$), and as in the short postPP spring program voles, this appeared to be due to a clamping down of *dio2* expression to background levels in 10 °C voles.

In contrast to *dio2*, *dio3* (Figure 5) appeared to be highly sensitive to postPP (spring: $F_{3,38} = 3.91$, $p = 0.02$, autumn: $F_{3,29} = 9.30$, $p < 0.001$) but insensitive to T_a . Within the spring-programmed voles, *dio3*

was detectable in LD10:14 and 12:12, but suppressed to background levels on the two longer postPPs. In autumn-programmed voles, *dio3* was detectable at longer photoperiods than in spring, with several individuals showing above baseline expression on LD14:10 and the following shorter photoperiods.

Somatostatin (Srif) Expression in the Arcuate Nucleus

Like with *dio2* and *dio3*, the sigmoid model fitted poorly on somatostatin expression, but an effect of postPP and T_a was clearly observable (Figure 6a, Table S2). In spring-programmed voles, somatostatin expression in response to postPP is T_a dependent with the higher T_a weakening the photoperiodic response ($T_a \times \text{postPP}$: $F_{3,32} = 4.703$, $p = 0.008$). By contrast, in

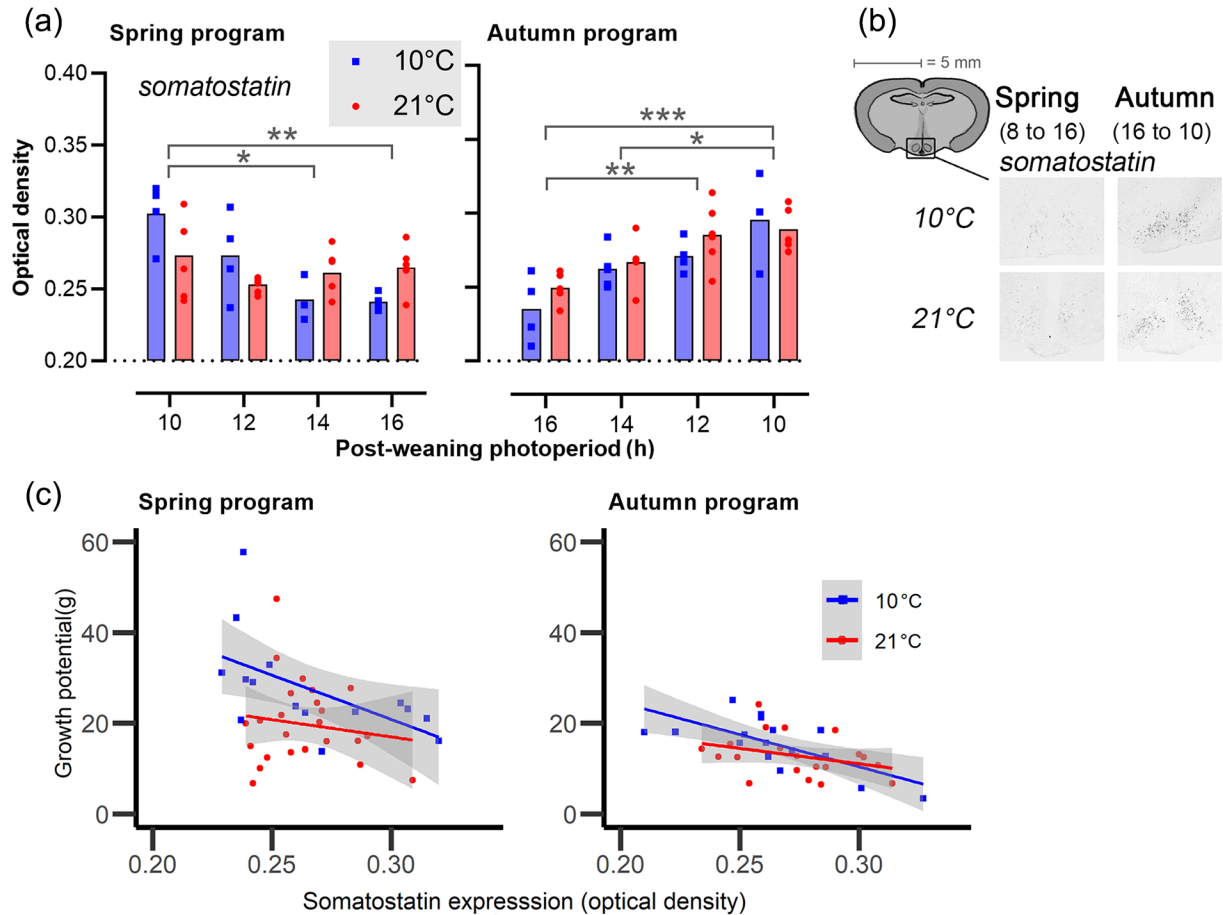


Figure 6. Expression of somatostatin (*srif*) in the arcuate nucleus. (a) Bar plots showing somatostatin expression in the arcuate nucleus. The left panels represent spring-programmed voles (gestated and raised to weaning under 8L) and the right panels represent autumn-programmed voles (gestated and raised to weaning under 16L) at 10 °C (blue squares) or 21 °C (red circles). (b) Representative images showing localization of mRNA by nonradioactive in situ hybridization in the arcuate nucleus. (c) Somatostatin (*srif*) expression (X-axis) against growth potential in g (Y-axis) for spring-programmed (left) and autumn-programmed (right) voles in which blue represents postweaning ambient temperatures of 10 °C and red at 21 °C. Gray areas indicate the 95% confidence levels of the regression line, and the data points are individual voles.

Significant effects are indicated: * $p < 0.05$. ** $p < 0.01$. *** $p < 0.001$.

autumn-programmed voles, photoperiodic effect on somatostatin expression was independent of T_a . In both groups, long postPPs had an inhibitory effect on somatostatin expression (spring: $F_{3,32} = 4.56$, $p = 0.009$; autumn: $F_{3,28} = 10.82$, $p < 0.001$).

Somatostatin expression across all postPPs did not significantly differ between spring-programmed (0.265 ± 0.004) and autumn-programmed (0.269 ± 0.004) voles or between ambient temperatures 10 °C (0.265 ± 0.005) and 21 °C (0.268 ± 0.003) across photoperiod treatments.

Growth in Response to Somatostatin Expression

Somatostatin expression in the arcuate nucleus was negatively correlated with the postweaning

growth potential in both spring-programmed ($F_{1,36} = 5.31$, $p = 0.03$) and autumn-programmed ($F_{1,32} = 14.51$, $p < 0.001$) voles (Figure 6b). Furthermore, low T_a (10 °C) in spring led to a significant increase in growth potential despite the growth-suppressive effect of somatostatin ($F_{1,36} = 7.10$, $p = 0.01$).

Gonadal Activation

The effects of photoperiod and T_a on gonadal weight and end-point plasma testosterone levels are summarized in Figure 7. Independent of gestational photoperiod and T_a , final gonadal weights in voles kept on a postPP of LD16:8 were consistently about 50% higher than the corresponding values in LD10:14 voles (spring, postPP: $F_{3,51} = 22.37$, $p < 0.001$;

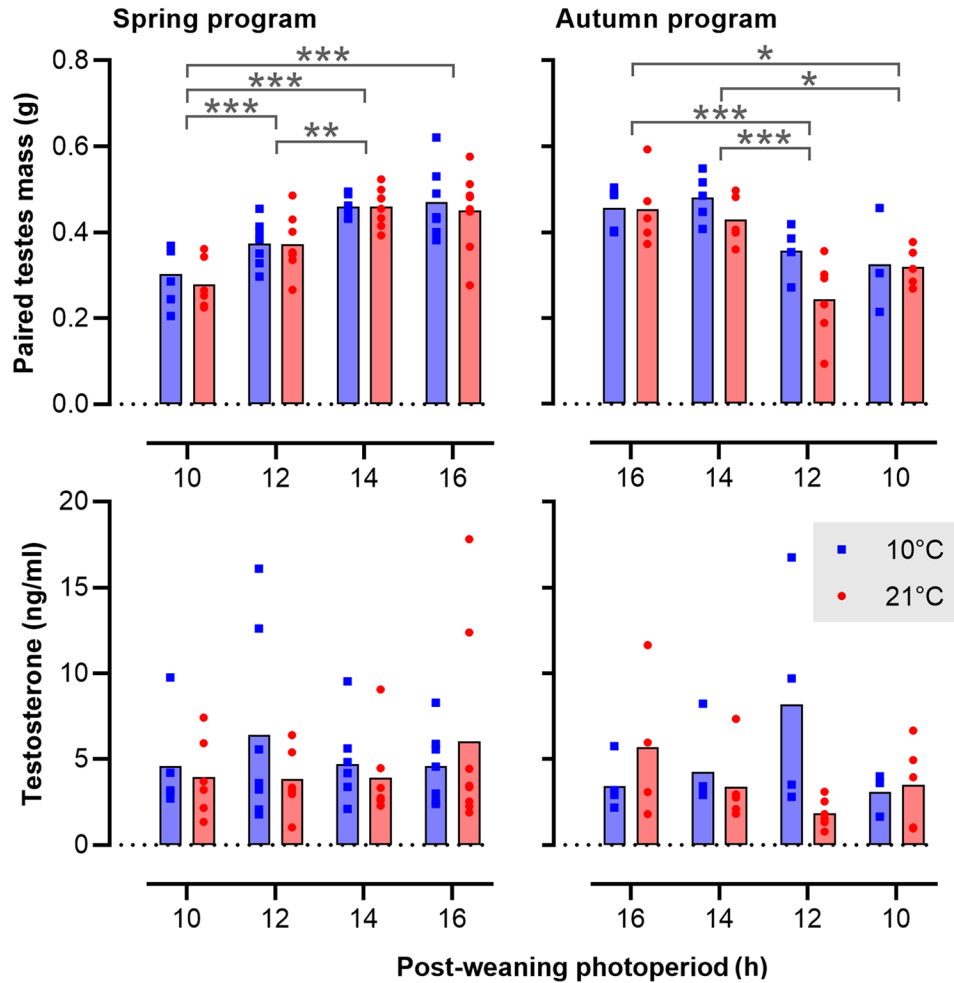


Figure 7. Activation of the gonadal axis in relation to photoperiod and ambient temperature. The bar plots show the mean and values for individual voles. The left panels represent spring-programmed voles (gestated and raised to weaning under 8L) and the right panels represent autumn-programmed voles (gestated and raised to weaning under 16L) at 10 °C (blue squares) or 21 °C (red circles). Abbreviation: ANOVA = analysis of variance. Data were log-transformed prior to analysis by two-way ANOVA. Significant effects are indicated: * $p < 0.05$. ** $p < 0.01$. *** $p < 0.001$.

autumn, postPP: $F_{3,30} = 12.18$, $p < 0.001$). Contrastingly, no significant effects of T_a on testicular growth were observed. Across the study as a whole, wide interindividual variation in testosterone levels at time of sacrifice was observed, and no significant effects of preweaning or postweaning conditions were found.

DISCUSSION

While there is a considerable literature on the programming effects of photoperiod on postnatal reproductive development in seasonal rodent species (Sáenz de Miera, 2019; van Dalum et al., 2020), few studies have focused on maternal photoperiodic programming of somatic growth (Horton, 2005). Here,

we have presented an analysis on this phenomenon in a microtine rodent in which effects on growth are at least as pronounced as those on reproductive development. Our data demonstrate that while gestational photoperiod does not affect body mass prior to weaning, it has a profound effect on postweaning growth parameters. Spring-programmed animals have a higher growth potential (i.e., the theoretical maximum size which an individual will attain) and a longer half-time (i.e., the time taken to attain 50% of the projected maximum weight) than do autumn-programmed animals. Since all animals had ad libitum access to food and water, and the *highest* body masses and growth potentials were seen in voles raised after weaning at a *low* ambient temperature (T_a), when thermoregulatory energy demands have been higher, we see photoperiodic history-dependent adoption of an autumn growth trajectory as a

programmed curtailment of the default summer growth trajectory. We suggest that this programming effect facilitates the redirection of dwindling autumn energy supplies toward overwintering survival and is the underlying cause of the numerous field observations of reduced body size linked to fitness in autumn born, overwintering cohorts of voles (Aars and Ims, 2002; Gliwicz, 1996; Zub et al., 2014). Indeed, the temperature effect on body mass disappeared when food was restricted and animals were not able to compensate high energy demands at low T_a by increasing food consumption (van Rosmalen and Hut, 2021a).

Low T_a enhanced growth potential to a greater extent in spring-programmed voles than in autumn-programmed voles. This asymmetry in the modulatory effect of T_a echoes field data on plasticity in the timing of pelage molt in snowshoe hares—where significant weather-dependent plasticity was seen in the completion of the spring but not the autumn molt (Zimova et al., 2014). From a functional perspective, increased programmed rigidity in autumn transitions might reflect high fitness costs of delaying preparation for winter based on unpredictable, and poorly predictive, benign autumn weather conditions. We are unclear as to why low T_a should increase growth potential in spring-programmed animals. Possibly low T_a in the spring condition signals that environmental conditions suitable for reproduction are likely to occur further into the future than in a warm spring, and this in turn encourages a commitment to investing in a large mature body size for later competitiveness. Against this hypothesis, and in contrast to our earlier observations in *M. arvalis* (van Rosmalen et al., 2020, 2021), we observed no corresponding disinvestment in the gonadal axis in low T_a spring animals; indeed, development of the gonadal axis in *M. oeconomus* appears to be entirely T_a insensitive and only mildly sensitive to photoperiodic influences (see also van Rosmalen et al., 2020, 2021). We have no data on core body temperature (T_b) or body composition (e.g., fat content) in this study but our previous study showed that T_b was lower at a T_a of 10 °C compared with 21 °C (van Rosmalen and Hut, 2021b) and another study showed that T_b correlates with T_a in tundra voles during the winter (Nieminen et al., 2013). The proportion of fat and de novo lipogenesis was not affected by photoperiod-induced body mass changes in *Microtus agrestis* (Król et al., 2005), *Lasiopodomys brandtii* (Li and Wang, 2005), and *M. oeconomus* (Wang et al., 2006), and an increased energy metabolism in winter suggests reliance on continuous food availability rather than fat accumulation in voles (Mustonen et al., 2002). Tundra voles may adapt behaviorally to cope with low temperatures through

huddling in tunnels dug under the snow (Korslund, 2006).

Analysis of *dio2/dio3* gene expression provides support for the notion that T_a , gestational and post-weaning photoperiodic influences converge at this level. In general terms, this view is consistent with the concept that the tanycyte cells in which the deiodinase genes are expressed are metabolic interfaces to the hypothalamic control systems (Bolborea and Dale, 2013; Dardente et al., 2014). In this study, the observed patterns of *dio2* and *dio3* were broadly consistent with those in the large body of published work describing the effects of seasonal status in the expression of these genes, with the spring condition being *dio2* dominant (*dio2* elevated, *dio3* suppressed) and vice versa in the autumn condition (Dardente et al., 2014; Hazlerigg and Simonneaux, 2015).

It is interesting to note that we observed T_a modulation of the expression of *dio2* but not *dio3*, and we therefore speculate that this may be the underlying cause of the asymmetry in the effect of T_a on growth potential: T_a modulates the *dio2*-dominant spring-programmed state, but not the *dio3*-dominant autumn-programmed state.

In Siberian hamsters, somatostatin (*srif*) expression in the arcuate nucleus shows inverse regulation to the annual body mass cycle (Petri et al., 2016) and treatment with the somatostatin agonist pasireotide mimics the effects of SP exposure on body mass and organ mass (Dumbell et al., 2015). We therefore wondered whether the observed effects of photoperiodic programming on growth parameters might be reflected in effects on *srif* gene expression. While we observed a weak negative correlation between arcuate *srif* expression and growth potential across all treatment groups (Figure 6b), the slope relationship did not change significantly as a function of photoperiodic treatment, and paradoxically we observed increased mean levels of *srif* expression in spring-programmed animals raised at low T_a , which had the highest overall growth potential. Since our sampling paradigm necessarily limited analysis of brain gene expression to the end of the study, we cannot exclude the possibility of *srif* involvement in growth programming in *M. oeconomus*.

Current models suggest that the regulation of *tsh β* gene expression in the PT represents the key photoperiodic switch for control of seasonal responses (Dardente et al., 2010; Masumoto et al., 2010), and is resistant to photoperiod-independent perturbatory effects—a resistance that might contribute to the function of the PT as a circannual calendar tissue (Lincoln et al., 2003; Wood and Loudon, 2018). In this light, we were surprised to observe a decrease in CP for suppression of *tsh β* expression in autumn-programmed animals held at low T_a . Given that neither

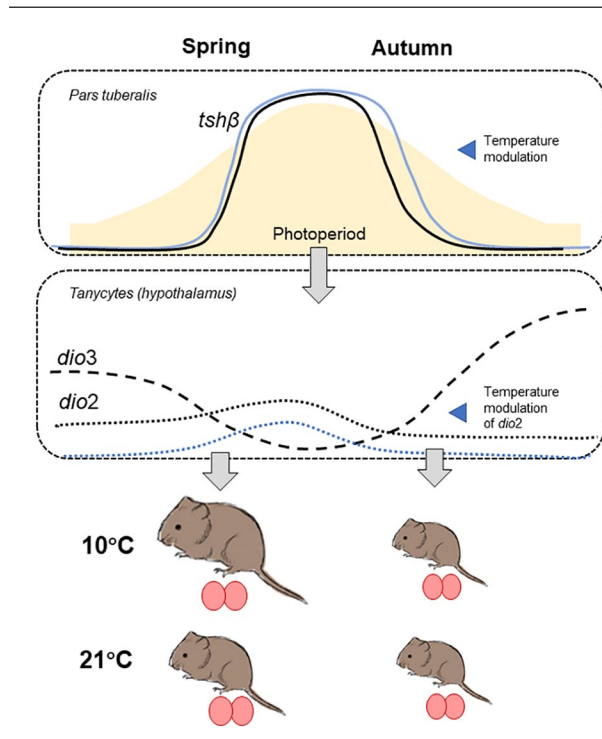


Figure 8. Summary of the photoperiod and temperature effects in tundra voles. *Tshβ* mRNA expression in the *pars tuberalis* follows photoperiod and shows a shift to a shorter (and thus later) critical photoperiod in autumn-programmed voles kept at 10 °C. Asymmetry in postweaning expression between spring and autumn programmed with only *dio2* responding to temperature in spring. This translated to increased growth potential in spring under 10 °C. Ovals indicate testes size which is insensitive to temperature changes and mildly responsive to postweaning photoperiod.

somatic growth potential nor gonadal weights show a similar pattern of response in autumn-programmed animals, it is difficult to put this finding in a functional context. Nevertheless, it raises the possibility that regulation of *tshβ* expression in the PT is more sensitive to metabolic influence than previously appreciated. Moreover, a previous study showed reduced *tshβ* expression in the PT of spring-programmed voles when food is scarce (van Rosmalen and Hut, 2021a).

In summary (Figure 8), this study characterizes the programming effect of early life photoperiod on somatic growth in tundra voles and shows that the plasticity of programming in the face of ambient temperature variation is greater in voles following a spring-type growth program. In the brain, this reflected in the temperature dependence of *dio2* gene expression in the mediobasal hypothalamus, and possibly *tshβ* expression in the PT, supporting the concept that this brain area is the key site for integration of metabolic status and calendar time. On a wider scope, our study provides new insights into temperature effects on the growth and reproductive axes of a high-latitude small herbivore. This may aid

understanding the adaptive potential of small mammals in the face of climate change and the rising temperatures at higher latitudes.

ACKNOWLEDGMENTS

The authors thank R. Schepers for his valuable help in tissue collections and animal care, Dr. H. Dardente for providing the probes for in situ hybridization, and Prof. Dr. M.P. Gerkema for establishing the common vole colony at the University of Groningen. This work was funded by the Adaptive Life program of the University of Groningen (Rijksuniversiteit Groningen, B050216 to L.v.R, R.T.M.R, L.d.W, and R.A.H) and by the Arctic University of Tromsø (Universitetet I Tromsø to M.J.v.D, D.A., F.C.M., and D.G.H). This work was also supported by grants from the Tromsø Research Foundation (TFS2016DH) and the Human Frontiers Science Program (RGP0030/2015) awarded to D.G.H.

CONFLICT OF INTEREST STATEMENT

The authors have no potential conflicts of interest with respect to the research, authorship, and/or publication of this article.

ORCID IDS

Mattis Jayme van Dalum  <https://orcid.org/0009-0006-0134-2389>

Laura van Rosmalen  <https://orcid.org/0000-0003-1273-1225>

NOTE

Supplementary material is available for this article online.

REFERENCES

- Aars J and Ims RA (2002) Intrinsic and climatic determinants of population demography: the winter dynamics of tundra voles. *Ecology* 83:3449-3456.
- Balčiauskas L, Balčiauskiene L, and Janonyte A (2012) Reproduction of the root vole (*Microtus oeconomus*) at the edge of its distribution range. *Turk J Zool* 36: 668-675.
- Bankhead P, Loughrey MB, Fernández JA, Dombrowski Y, McArt DG, Dunne PD, McQuaid S, Gray RT, Murray

- LJ, Coleman HG, et al. (2017) QuPath: open source software for digital pathology image analysis. *Sci Rep* 7: 1-7.
- Bolborea M and Dale N (2013) Hypothalamic tanycytes: potential roles in the control of feeding and energy balance. *Trends Neurosci* 36:91-100.
- Bronson FH (1985) Mammalian reproduction: an ecological perspective. *Biol Reprod* 32:1-26.
- Bronson FH (1988) Mammalian reproductive strategies: genes, photoperiod and latitude. *Reprod Nutr Dev* 28:335-347.
- Bronson FH (2009) Climate change and seasonal reproduction in mammals. *Philos Trans R Soc Lond B* 364: 3331-3340.
- Brunhoff C, Galbreath KE, Fedorov VB, Cook JA, and Jaarola M (2003) Holarctic phylogeography of the root vole (*Microtus oeconomus*): implications for late Quaternary biogeography of high latitudes. *Mol Ecol* 12:957-968.
- Conroy CJ and Cook JA (2000) Phylogeography of a post-glacial colonizer: *Microtus longicaudus* (Rodentia: Muridae). *Mol Ecol* 9:165-175.
- Dardente H, Hazlerigg DG, and Ebling FJ (2014) Thyroid hormone and seasonal rhythmicity. *Front Endocrinol (Lausanne)* 5:19-11.
- Dardente H, Wyse CA, Birnie MJ, Dupré SM, Loudon ASI, Lincoln GA, and Hazlerigg DG (2010) A molecular switch for photoperiod responsiveness in mammals (supplemental information). *Curr Biol* 20:2193-2198.
- Dumbell RA, Scherbarth F, Diedrich V, Schmid HA, Steinlechner S, and Barrett P (2015) Somatostatin agonist pasireotide promotes a physiological state resembling short-day acclimation in the photoperiodic male Siberian hamster (*Phodopus sungorus*). *J Neuroendocrinol* 27:588-599.
- Eccard JA and Herde A (2013) Seasonal variation in the behaviour of a short-lived rodent. *BMC Ecol* 13:43.
- Ergon T (2007) Optimal onset of seasonal reproduction in stochastic environments: when should overwintering small rodents start breeding? *Ecoscience* 14:330-346.
- Ergon T, MacKinnon JL, Stenseth NC, Boonstra R, and Lambin X (2001) Mechanisms for delayed density-dependent reproductive traits in field voles, *Microtus agrestis*: the importance of inherited environmental effects. *Oikos* 95:185-197.
- Gliwicz J (1996) Life history of voles: growth and maturation in seasonal cohorts of the root vole. *Misc Zool* 19: 1-12.
- Gliwicz J (2007) Increased reproductive effort as a life history response of *Microtus* to predation. *Ecoscience* 14:314-317.
- Hazlerigg D and Simonneaux V (2015) Seasonal regulation of reproduction in mammals. In: Plant TM and Zeleznik AJ, editors. *Knobil and Neill's Physiology of Reproduction (Fourth Edition)*. Academic Press, p. 1575-1604. <https://doi.org/10.1016/C2011-1-07288-0>
- Herwig A, Petri I, and Barrett P (2012) Hypothalamic gene expression rapidly changes in response to photoperiod in juvenile Siberian hamsters (*Phodopus sungorus*). *J Neuroendocrinol* 24:991-998.
- Horton TH (2005) Fetal origins of developmental plasticity: animal models of induced life history variation. *Am J Hum Biol* 17:34-43.
- Horton TH and Stetson MH (1992) Maternal transfer of photoperiodic information in rodents. *Anim Reprod Sci* 30:29-44.
- Jaarola M, Martínková N, Gündüz I, Brunhoff C, Zima J, Nadachowski A, Amori G, Bulatova NS, Chondropoulos B, Fraguadakis-Tsolis S, et al. (2004) Molecular phylogeny of the speciose vole genus *Microtus* (Arvicolinae, Rodentia) inferred from mitochondrial DNA sequences. *Mol Phylogenet Evol* 33:647-663.
- Korslund L (2006) Activity of root voles (*Microtus oeconomus*) under snow: social encounters synchronize individual activity rhythms. *Behav Ecol Sociobiol* 61:255-263.
- Kriegsfeld LJ, Trasy AG, and Nelson RJ (2000) Temperature and photoperiod interact to affect reproduction and GnRH synthesis in male prairie voles. *J Neuroendocrinol* 12:553-558.
- Król E, Redman P, Thomson PJ, Williams R, Mayer C, Mercer JG, and Speakman JR (2005) Effect of photoperiod on body mass, food intake and body composition in the field vole, *Microtus agrestis*. *J Exp Biol* 208:571-584.
- Lenth RV (2016) Least-squares means: the R package lsmeans. *J Stat Softw* 69:1-33.
- Li XS and Wang DH (2005) Regulation of body weight and thermogenesis in seasonally acclimatized Brandt's voles (*Microtus brandti*). *Horm Behav* 48:321-328.
- Lincoln GA, Andersson H, and Loudon A (2003) Clock genes in calendar cells as the basis of annual timekeeping in mammals: a unifying hypothesis. *J Endocrinol* 179:1-13.
- Lomet D, Cagnié J, Chesneau D, Dubois E, Hazlerigg D, and Dardente H (2018) The impact of thyroid hormone in seasonal breeding has a restricted transcriptional signature. *Cell Mol Life Sci* 75:905-919.
- Masumoto KH, Ukai-Tadenuma M, Kasukawa T, Nagano M, Uno KD, Tsujino K, Horikawa K, Shigeyoshi Y, and Ueda HR (2010) Acute induction of Eya3 by late-night light stimulation triggers TSH β expression in photoperiodism. *Curr Biol* 20:2199-2206.
- Mustonen AM, Nieminen P, and Hyvärinen H (2002) Melatonin and the wintering strategy of the tundra vole, *Microtus oeconomus*. *Zool Sci* 19:683-687.
- Nieminen P, Hohtola E, and Mustonen AM (2013) Body temperature rhythms in *Microtus* voles during feeding, food deprivation, and winter acclimatization. *J Mammal* 94:591-600.
- Petri I, Diedrich V, Wilson D, Fernandez-Calleja J, Herwig A, Steinlechner S, and Barrett P (2016) Orchestration of gene expression across the seasons: hypothalamic

- gene expression in natural photoperiod throughout the year in the Siberian hamster. *Sci Rep* 6:1-9.
- Ritz C, Baty F, Streibig JC, and Gerhard D (2015) Dose-response analysis using R. *PLoS ONE* 10:1-13.
- RStudio Team (2020) Rstudio: Integrated development for R. R Studio. [accessed 2023 April 16]. <http://www.rstudio.com>.
- Sáenz de Miera C (2019) Maternal photoperiodic programming enlightens the internal regulation of thyroid-hormone deiodinases in tanycytes. *J Neuroendocrinol* 31:e12679.
- Tast J (1966) The root vole, *Microtus oeconomus* (Pallas) as an inhabitant of seasonally flooded land. *Annales Zoologici Fennici* 3:127-171.
- van Dalum J, Melum VJ, Wood SH, and Hazlerigg DG (2020) Maternal photoperiodic programming: melatonin and seasonal synchronization before birth. *Front Endocrinol* 10:1-7.
- van de Zande L, van Apeldoorn RC, Blijdenstein AF, de Jong D, van Delden W, and Bijlsma R (2000) Microsatellite analysis of population structure and genetic differentiation within and between populations of the root vole, *Microtus oeconomus* in the Netherlands. *Mol Ecol* 9:1651-1656.
- van Rosmalen L and Hut RA (2021a) Food and temperature change photoperiodic responses in two vole species. *J Exp Biol* 224:jeb.243030.
- van Rosmalen L and Hut RA (2021b) Negative energy balance enhances ultradian rhythmicity in spring-programmed voles. *J Biol Rhythms* 36:359-368.
- van Rosmalen L, van Dalum J, Appenroth D, Roodenrijs RTM, deWit L, Hazlerigg DG, and Hut RA (2021) Mechanisms of temperature modulation in mammalian seasonal timing. *FASEB J* 35:e21605-12.
- van Rosmalen L, van Dalum J, Hazlerigg DG, and Hut RA (2020a) Gonads or body? Differences in gonadal and somatic photoperiodic growth response in two vole species. *J Exp Biol* 223:jeb.230987.
- van Rosmalen L, van Dalum J, Hazlerigg DG, and Hut RA (2020b) Gonads or body? Differences in gonadal and somatic photoperiodic growth response in two vole species. *J Exp Biol* 223:jeb.230987.
- Visser ME, Caro SP, van Oers K, Schaper SV, and Helm B (2010) Phenology, seasonal timing and circannual rhythms: towards a unified framework. *Phil Trans Royal Soc B* 365:3113-3127.
- Visser ME, Holleman LJM, and Caro SP (2009) Temperature has a causal effect on avian timing of reproduction. *Proc Royal Soc B* 276:2323-2331.
- Wang JM, Zhang YM, and Wang DH (2006) Photoperiodic regulation in energy intake, thermogenesis and body mass in root voles (*Microtus oeconomus*). *Comp Biochem Physiol A Mol Integr Physiol* 145:546-553.
- Wickham H, Averick M, Bryan J, Chang W, McGowan L, François R, Golemund G, Hayes A, Henry L, Hester J, et al. (2019) Welcome to the tidyverse. *Journal of Open Source Softw* 4:1686.
- Wood S and Loudon A (2018) The pars tuberalis: the site of the circannual clock in mammals? *Gen Comp Endocrinol* 258:222-235.
- Zimova M, Mills LS, Lukacs PM, and Mitchell MS (2014) Snowshoe hares display limited phenotypic plasticity to mismatch in seasonal camouflage. *Proc Royal Soc B* 281:20140029.
- Zub K, Borowski Z, Szafrńska PA, Wiczorek M, and Konarzewski M (2014) Lower body mass and higher metabolic rate enhance winter survival in root voles, *Microtus oeconomus*. *Biol J Linnean Soc* 113:297-309.